Soft Matter

Accepted Manuscript

ROYAL SOCIETY OF CHEMISTRY

www.rsc.org/softmatter

Journal Name

ARTICLE TYPE

Cite this: DOI: 10.1039/xxxxxxxxxx

Configurable lipid membrane gradients quantify diffusion, phase separations and binding densities†

Katherine N. Liu,[ab] Chen-min S. Hung,[ac] Michael A. Swift,[ac] Kristen A. Muñoz,[ac] Jose L Cortez ,[ad] and Babak Sanii*[abcd]

Received Date
Accepted Date

DOI: 10.1039/xxxxxxxxxx

www.rsc.org/journalname

Single-experiment analysis of phospholipid compositional gradients reveals diffusion coefficients, phase separation parameters, and binding densities as a function of localized lipid mixture. Compositional gradients are formed by directed self assembly where rapid-prototyping techniques (i.e., additive manufacturing or laser-cutting) prescribe lipid geometries that self-spread, heal and mix by diffusion.

Phospholipid membranes adhering to solid substrates are widely used to study thin-film material properties and as simplified model systems for biological membranes[1–5]. Solid supported lipid bilayers (SSLB) retain aspects of biological membranes, they are molecularly thick and can have a broad range of functionalities and compositions[3]. Other aspects are impinged; for example, lateral diffusion is typically reduced compared to free-membranes[6], and some membrane proteins will not functionally insert in SSLB. However, SSLBs also enable capabilities such as array-based interfacing by photolithographic/microcontact/microfluidic patterning[7,8]. Their scalable lateral extent allows applications such as tunable lubrication layers[9], filtration devices[10], and as part of lab-on-a-chip healthcare/environmental-monitoring biosensors[11,12]. Additionally, their substrates can incorporate functionalities such as tethering to enable greater trans-membrane protein insertion[11] and conductivity for direct electrical measurements[13].

Both the material science and biomimetic aspects of membranes are strongly influenced by the composition of phospholipids[14–16], and would benefit from greater compositional and spatial control capabilities. Typically, to systematically vary the composition of SSLBs requires separate lipid depositions in distinct experiments or bins[17–19]. An appealing alternative would be to characterize a single membrane compositional gradient as it equilibrates.

Membrane gradients of a broad range of lipid compositions can be formed by adapting a lipid spreading‡ membrane deposition approach. Lipid spreading occurs spontaneously when a multilayer lipid stack on a hydrophilic[20,21] or hydrophobic[22] surface is hydrated at a temperature above its fluid phase transition temperature (see Fig. 1BC). A membrane extends from the lipid stack with a rate proportional to the square-root of time, energetically driven by substrate interactions and phospholipid reorganization[23]. On hydrophilic surfaces the extending membrane is a molecular bilayer, as confirmed by imaging ellipsometry[22,24]. When two such bilayers meet they self-heal into one contiguous membrane[25] and mix (Fig. 1B).

Here, we use equilibrating membrane gradients to measure diffusion coefficients, phase separations and binding densities as a function of lipid composition. We report configurable methods to produce membrane collisions that self-assemble into phospholipid gradients. The directed self-assembly methods do not require micro-machining and are rapidly configurable. We char-

[a] Keck Science Department, Claremont, CA USA, bsanii@kecksci.claremont.edu
[b] Scripps College
[c] Claremont McKenna College
[d] Pitzer College

† Electronic Supplementary Information (ESI) available: Stamp specifications, domain-formation conditions, D measurement sensitivity, video of collision. See DOI: 10.1039/b000000x/

‡ Lipid spreading is sometimes used to describe membrane deposition by vesicle-fusion. Here we use it to describe lipids spreading from a surface-adhering stack.

acterize post-collision mixing to generate convenient experimental parameters, and we apply the system to perform preliminary studies on non-equilibrated membranes. We find that the equilibration is nominally diffusive, and occurs on experimentally accessible time- and length- scales.

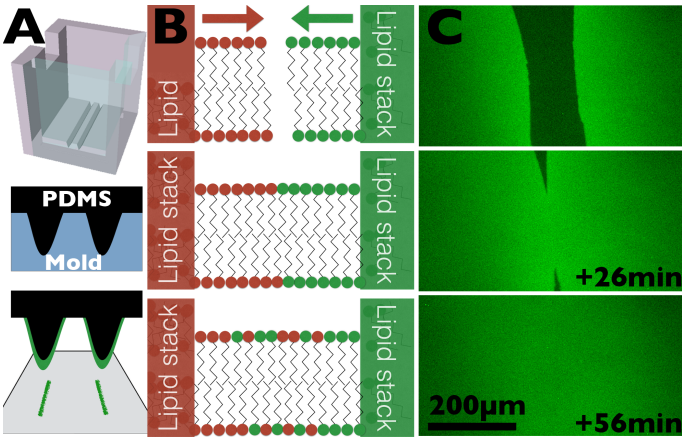

Fig. 1 (A, top to bottom) Diagram of 3D printed mold; molding a PDMS stamp; stamping lipid geometry (B) Diagram of lipids from apposed multilayer sources spreading, colliding/self-healing and mixing. (C) Selected false-color fluorescence images from a video of collision of POPC bilayers with sources 0.85 mm apart, both doped with 3% NBD-DHPE. Frames are 65, 91, and 121 minutes after sample immersion in buffer. Full video in SI†.

We collide our membranes by lipid spreading as the approach is not limited to charged lipids[26] or by lipid headgroup-drag considerations[27,28]. Additionally, lipid stacks can be configured in geometries without the need for microfabrication techniques[29]. We prescribed the membrane collisions by adapting rapid prototyping approaches. Molds were digitally designed with depressed features where lipid deposition was desired (e.g., Fig 1A), and manufactured with either a consumer-grade 3D printer (Afinia H480) or a consumer-grade laser-cutter (Full Spectrum Engineering H-series). Printing and cutting parameters are included in SI†. Stamps were formed by curing poly(dimethylsiloxane) (PDMS, Dow Corning Sylgard 184) in the molds for two hours at 80°C, and then rinsed with ethanol. 1-5 μL of ethanol/phospholipid (Avanti Polar Lipids) solutions (7.5 mg/mL) were manually deposited on each raised surface of the stamp by syringe (Hamilton 1701 RN), and placed in dark vacuum for at least two hours prior to use. Stamps were manually pressed onto plasma-etched (Harrick, PDC-32G, 4 minutes in air/vacuum) glass cover-slips to transfer phospholipid stacks in the geometries prescribed by the molds. Samples were subsequently hydrated in petri dishes with 3-4 mL of Phosphate Buffered Saline (PBS, 10mM phosphate buffer, 2.7mM KCl, 137mM NaCl, pH 7.4, Bioland Scientific LLC). Samples were imaged with a custom fluorescence microscope, and labeled with N-(7-Nitrobenz-2-oxa-1,3-diazol-4-yl)-1,2-dihexadecanoyl-snglycero-3-phosphoethanolamine, triethylammonium salt (NBD-DHPE, Biotium), N-(Texas Red sulfonyl)-1,2-dihexadecanoyl-snglycero-3-phosphoethanolamin, triethylammonium salt (Texas Red-DHPE, Biotium) and/or Streptavidin Texas-Red conjugate (Life Technologies). Data analysis was performed with Fiji[30] and Octave[31].

Intensity profiles of an asymmetrical collision where only one side fluoresces can be analyzed to determine the diffusion coefficient (Fig. 2). We fit intensity profiles to a model of phospholipid diffusion per Fick's second law[32] ($D\frac{\partial^2 C}{\partial x^2} = \frac{\partial C}{\partial t}$, where D is the diffusion coefficient, C is the concentration of fluorophores, and x/t are the spatial/temporal extents). At the moment of collision, the initial condition of fluorescence intensity is approximated as a step function§ (see SI†). Solving the fluorophore concentration and including intensity-offset and scaling terms produces a fit function[33] for our data:

$$C(x,t) = A \times \mathrm{erf}\left(\frac{x - x_o}{2\sqrt{Dt}}\right) + offset \qquad (1)$$

We fit the intensity profile at each time-point to equation 1 by non-linear least-squares fitting[34] (Fig. 2A) to determine the fit parameters of amplitude (A), offset, diffusion coefficient (D), collision midpoint (xo) and fit time (t). The D and t fit variables are not independent, and they are often combined in a single fit term, the diffusion length ($\sqrt{Dt}$). The slope of the diffusion-length squared (D*t) versus the known sampling time is the diffusion coefficient (Fig 2B).

For a collision of 1-palmitoyl-2-oleoyl-sn-glycero-3-phosphocholine (POPC) and POPC with 3% NBD-DHPE, we measured a diffusion coefficient of $2.4 \mu m^2/s$. The line was measurable and linear, thus consistent with diffusion at time-scales of over an hour. The diffusion value is in rough agreement with literature values of POPC on glass[35], though a broad range of literature diffusion values are reported possibly due to variations in glass surface roughness and cleaning techniques[36]. This approach to measure diffusion coefficients is relatively insensitive to variations in the angle and placement of the intensity profile in a single sample (see SI†).

The spacing between the lipid stacks (d) is a key experimental parameter. A wider spacing corresponds to a longer delay before collision and gradient formation ($t \propto d^2/\beta$, β is the kinetic spreading coefficient[21]). A closer spacing limits the time before the width of the gradient is impinged by the stacks, which complicates analysis ($t \propto d^2/D$). These competing considerations benefit from optimization for different lipid compositions (i.e., different

§ Not all fluorophores approximate step-functions at the moment of collision, as partitioning can occur during spreading. For example, TR-DHPE accumulates during spreading, though relaxes quickly after the collision. Strongly partitioning fluorophores will require analysis with different initial conditions.

β and D), which is more convenient with our rapid prototyping techniques than with micro-fabrication. We found that a deposition geometry of apposed lines 0.75-1 mm apart produces a collision between spreading POPC bilayers approximately 60-120 minutes after hydration at room temperature. The configurable delay between hydration and collision is convenient for positioning the system to image the collision and subsequent mixing. An additional consideration is that the brightness of multilayer stacks can obscure images of the area of collision, so the distance between apposed stacks was set to be larger than the microscope's field of view.

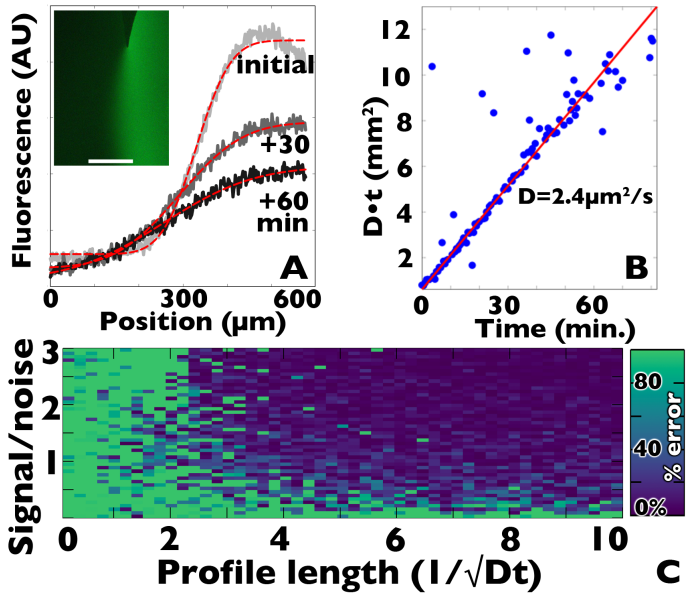

Fig. 2 (A) Fluorescence intensity profiles across a collision of unlabeled POPC bilayer on the left with 97% POPC / 3% NBD-DHPE on the right at select time points, along with fits to equation 1. Inset: image of collision in progress, 200μm scalebar. (B) The fit diffusion length squared (Dt) vs. (t) along with a robust linear fit. (C) Fitting equation 1 to synthetic data. Signal/noise is defined as amplitude (A) divided by amplitude of added pseudorandom noise. Profile length is in units of diffusion lengths. Fitting is by Nelder and Mead Simplex algorithm[34] (1500 maximum function evaluations, and an iteration tolerance of 10^{-6})

The linearity of the measured diffusion length vs. time plot (Fig. 2B) indicates a consistent diffusion coefficient over the hour-long measurement, although 63% photobleaching occurred in that time. This method's resiliency to photobleaching is due to the diffusion length term ($\sqrt{Dt}$) being distinct from the amplitude and offset terms in equation 1. We computationally tested the robustness of this method by generating an ideal dataset of profiles of a known diffusion-length, but with varying amplitude/noise ratios and profile lengths. The fit diffusion length is accurately recovered for a broad range of amplitude-to-noise ratios greater than one (see Fig. 2C). If the length of the measured profile relative to the diffusion length is too small (< a factor of 4), then one is fitting just the center of the erf function far from the "shoulders", which can produce ambiguous fits. We can estimate the experimental timeframe by equating the field of view with 4 times the diffusion length. For POPC ($2.4\mu m^2/s$) and an imaging width of a 500 μm, this suggests an experimental timeframe of measurable mixing of over an hour (6510s).

Gradients produced at this configuration have conveniently long (>1 hour) equilibration times, with diffusion lengths on the order of mm. In comparison, local lipid interactions are on the order of μm[37], and diffusion is on the order of $\mu m^2/s$. That is, lipids locally quasi-equilibrate on the orders of seconds, while macroscopically the gradient dynamically equilibrates over thousands of seconds. We can thus treat snapshots along the equilibrium path of the gradient as quasi-equilibrated states. This approach enables a powerful method of studying the effects of multiple membrane compositions from a single image. The spatial extent along the axis of mixing is used to determine the composition of the membrane at that point. We demonstrate the versatility of this approach with two compositionally-sensitive applications: domain formation and protein binding densities.

Galactosylceramide(GalCer.)/cholesterol(Chol.)/ POPC is a model domain-forming lipid mixture of biological importance[38,39]. Domains were formed on a compositional gradient (Fig. 3A) after a heating and slow-cooling cycle[40] (see SI†). Using fluorescence intensity as an approximate proxy for membrane composition, we quantified domain properties as a function of local lipid composition. In particular, two distinct co-existing populations of domains were identified: a larger dendritic domain and a smaller circular domain. The dendritic domains correspond to GalCer and cholesterol concentrations in excess of 24% and 7% respectively. Increased cholesterol has been suggested to reduce domain line tension[41]; we are currently exploring this phenomenon further with gradients of each component. A symmetrical collision between identical domain-forming compositions does not produce a gradient in domain characteristics (see SI†).

Protein binding can also be sensitive to local lipid compositions, and is assayable with such membrane gradients. We formed a gradient of a 93/7% mixture of POPC/ 1,2-Dipalmitoyl-sn-Glycero-3-Phosphoethanolamine-N-(Biotinyl) to a 97/3% mixture of POPC/NBD-DHPE. Biotin-streptavidin binding is a common linking motif in bioengineering. The gradient was incubated in a 2μg/mL solution of fluorescent Texas-Red conjugated streptavidin protein for 15 minutes before rinsing with PBS buffer and imaging with a fluorescence microscope. Intensity profiles from images filtered for NBD-DHPE are fit to equation 1 and normalized to estimate the localized percentage of biotinylated lipids. Intensity profiles filtered for Texas-Red estimate the local irreversible binding of streptavidin. Plotting these two quantities against each other reveals streptavidin binding density as a

function of biotin density (Fig. 3B). These data illustrate linear loading that saturates at 1.5% biotinylated lipids, in rough agreement with published data of biotinylated lipids in a 1,2-dilauroyl-sn-glycero-3-phosphocholine (DLPC) membrane[42]. Notably, the previous study reported loading at 7 different biotin concentrations from at least that many distinct membranes, whereas this technique determined loading at 330 biotin concentrations from a single sample.

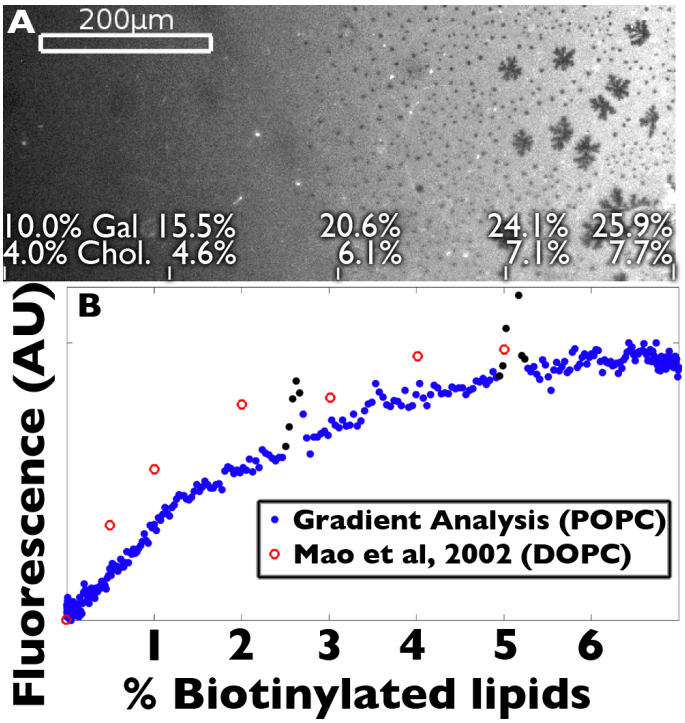

Fig. 3 Applications of lipid composition gradients. (A): Gradient of domain-forming lipid compositions resulting from a collision of 97/3% POPC/NBD-DHPE with 64/27/8/1% POPC/GalCer/Chol/TR-DHPE. Listed compositions were determined by TR-DHPE intensity-fitting to Equation 1. (B) Fluorescent streptavidin binding density as a function of % biotinylated lipids in POPC, determined from a single gradient-binding experiment. Peaks at 3 and 5% correspond to anomalous vesicles adhered to the membrane (shown in black). Data is in agreement with a similar multiple-experiment streptavidin binding assay to biotinylated lipids, shown in red. (Adapted with permission from reference 34. Copyright 2002 American Chemical Society.)

In summary, we find that membrane gradients produced by spreading and colliding lipids equilibrate by diffusion. The experimentally accessible diffusion-lengths and equilibration-times are amendable to quasi-equilibrium studies to quantify diffusion, phase behavior and protein binding. For example, single experiments determined that streptavidin loading begins saturating at 1.5% biotinylated lipids, and that distinct co-existing domains exist at concentrations above 24/7% GalCer/cholesterol, both in POPC. Additionally, we introduce and characterize a simplified method for producing and analyzing configurable membrane gradients. While we measured our gradients with fluorescence intensities, this approach is not limited to fluorescence and can readily be extended to a variety of approaches including imaging ellipsometry[24], imaging mass spectroscopy[43], and atomic force microscopy[44]. Also, we primarily studied one-dimensional gradients across a planar membrane collision. However, the rapid-prototyping aspect of this approach facilitates a broad range of collision geometries that enable studies such as three-way mixing and radial self-healing. An exciting prospect of this platform is that it could be used to study non-diffusive molecular transport between dissimilar lipid bilayers.

Acknowledgements KL, CH, and JC were supported by Howard Hughes Medical Institute (HHMI) Student Summer Fellowships, KM by Rose Hills Foundation Funding, and MS by the Keck Foundation Summer Research Fellowship. We thank K. Black and R. Levy for thoughtful discussions, S. Walt and N. Smith for the colormap used in 2C, as well as Z. Tang, N. Copp, A.N. Parikh, K. Nguyen, V. Nguyen and W. Cook for insight, instrumentation and expertise.

References

1 I. Czolkos, A. Jesorka and O. Orwar, *Soft Matter*, 2011, **7**, 4562–4576.
2 A. N. Parikh and J. T. Groves, *MRS Bulletin*, 2006, **31**, 507–512.
3 E. Sackmann, *Science*, 1996, **271**, 43–48.
4 A. Grakoui, S. K. Bromley, C. Sumen, M. M. Davis, A. S. Shaw, P. M. Allen and M. L. Dustin, *Science*, 1999, **285**, 221–227.
5 H. Bayley and P. S. Cremer, *Nature*, 2001, **413**, 226–230.
6 M. Przybylo, J. Sýkora, J. Humpolíčková, A. Benda, A. Zan and M. Hof, *Langmuir*, 2006, **22**, 9096–9099.
7 A. Ainla, I. Gözen, B. Hakonen and A. Jesorka, *Scientific reports*, 2013, **3**, 1–6.
8 E. T. Castellana and P. S. Cremer, *Surface Science Reports*, 2006, **61**, 429–444.
9 C. Liu, M. Wang, J. An, E. Thormann and A. Dėdinaitė, *Soft Matter*, 2012, **8**, 10241–10244.
10 Y. Kaufman, A. Berman and V. Freger, *Langmuir*, 2010, **26**, 7388–7395.
11 J. A. Jackman, W. Knoll and N.-J. Cho, *Materials*, 2012, **5**, 2637–2657.
12 D. Grieshaber, R. MacKenzie, J. Voeroes and E. Reimhult, *Sensors*, 2008, **8**, 1400–1458.
13 G. Wiegand, N. Arribas-Layton, H. Hillebrandt, E. Sackmann and P. Wagner, *The Journal of Physical Chemistry B*, 2002, **106**, 4245–4254.
14 J. E. C. Jr and E. P. Gelmann, *Bacteriological Reviews*, 1975, **39**, 256.
15 G. V. Meer, D. R. Voelker and G. W. Feigenson, *Nature Reviews Molecular Cell Biology*, 2008, **9**, 112–124.
16 M. Bloom, E. Evans and O. G. Mouritsen, *Quarterly reviews of biophysics*, 1991, **24**, 293–397.
17 L. Kam and S. G. Boxer, *Journal of the American Chemical Society*, 2000, **122**, 12901–12902.
18 J. T. Groves, L. K. Mahal and C. R. Bertozzi, *Langmuir*, 2001, **17**, 5129–5133.
19 J. S. Hovis and S. G. Boxer, *Langmuir*, 2001, **17**, 3400–3405.
20 J. Rädler, H. Strey and E. Sackmann, *Langmuir*, 1995, **11**, 4539–4548.
21 J. Nissen, S. Gritsch, G. Wiegand and J. O. Rädler, *The European Physical Journal B-Condensed Matter and Complex Systems*, 1999, **10**, 335–344.
22 B. Sanii and A. N. Parikh, *Soft Matter*, 2007, **3**, 977.
23 B. Sanii, K. Nguyen, J. O. Rädler and A. N. Parikh, *ChemPhysChem*, 2009, **10**, 2787–2790.
24 M. C. Howland, A. W. Szmodis, B. Sanii and A. N. Parikh, *Biophysical journal*, 2007, **92**, 1306–1317.
25 J. Nissen, K. Jacobs and J. O. Rädler, *Physical Review Letters*, 2001, **86**, 1904–1907.
26 J. T. Groves and S. G. Boxer, *Biophysical journal*, 1995, **69**, 1972–1975.
27 L. Chao and S. Daniel, *Journal of the American Chemical Society*, 2011, **133**, 15635–15643.

28 P. Jönsson, J. P. Beech, J. O. Tegenfeldt and F. HÃűÃűk, *Journal of the American Chemical Society*, 2009, **131**, 5294–5297.

29 K. Furukawa, H. Nakashima, Y. Kashimura and K. Torimitsu, *Langmuir*, 2008, **24**, 921–926.

30 J. Schindelin, I. Arganda-Carreras, E. Frise, V. Kaynig, M. Longair, T. Pietzsch, S. Preibisch, C. Rueden, S. Saalfeld, B. Schmid, J.-Y. Tineves, D. J. White, V. Hartenstein, K. Eliceiri, P. Tomancak and A. Cardona, *Nature Methods*, 2012, **9**, 676–682.

31 J. W. Eaton, D. Bateman, S. Hauberg and R. Wehbring, 2015.

32 A. Fick, *The London, Edinburgh, and Dublin Philosophical Magazine and Journal of Science*, 1855, **10**, 30–39.

33 J. Crank, *The Mathematics of Diffusion*, Oxford University Press, 1979.

34 J. A. Nelder and R. Mead, *The Computer Journal*, 1965, **7**, 308–313.

35 W. L. Vaz, R. M. Clegg and D. Hallmann, *Biochemistry*, 1985, **24**, 781–786.

36 K. J. Seu, A. P. Pandey, F. Haque, E. A. Proctor, A. E. Ribbe and J. S. Hovis, *Biophysical journal*, 2007, **92**, 2445–2450.

37 A. M. Smith, M. Vinchurkar, N. Gronbech-Jensen and A. N. Parikh, *Journal of the American Chemical Society*, 2010, **132**, 9320–9327.

38 C. D. Blanchette, W.-C. Lin, C. A. Orme, T. V. Ratto and M. L. Longo, *Biophysical Journal*, 2008, **94**, 2691–2697.

39 C. D. Blanchette, W.-C. Lin, T. V. Ratto and M. L. Longo, *Biophysical Journal*, 2006, **90**, 4466–4478.

40 C. Wang, M. R. Krause and S. L. Regen, *JACS Communication*, 2015, **137**, 664–666.

41 W.-C. Lin, C. D. Blanchette and M. L. Longo, *Biophysical journal*, 2007, **92**, 2831–2841.

42 H. Mao, T. Yang and P. S. Cremer, *Analytical Chemistry*, 2002, **74**, 379–385.

43 M. M. Lozano, Z. Liu, E. Sunnick, A. Janshoff, K. Kumar and S. G. Boxer, *Journal of the American Chemical Society*, 2013, **135**, 5620–5630.

44 L. Picas, F. Rico and S. Scheuring, *Biophysical journal*, 2012, **102**, L01–L03.

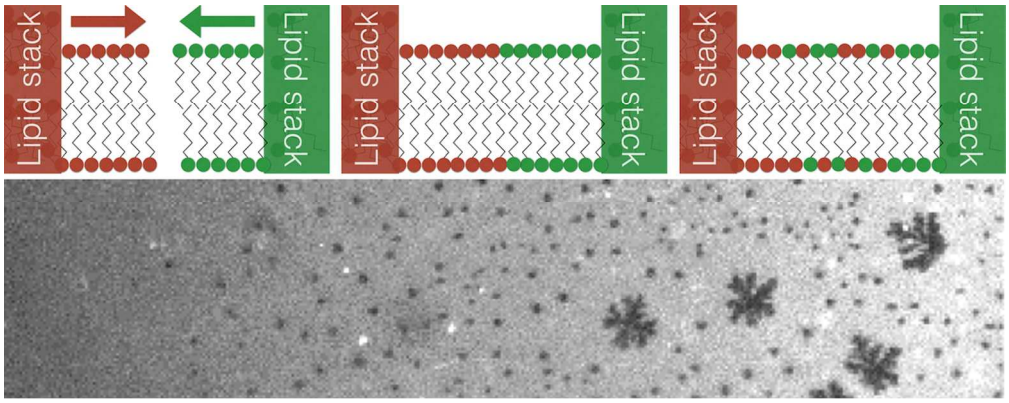

Tunable collisions between spreading phospholipid membranes form functional gradients.